



This discussion paper is/has been under review for the journal Atmospheric Chemistry and Physics (ACP). Please refer to the corresponding final paper in ACP if available.

# Constraining the $\text{N}_2\text{O}_5$ UV absorption cross-section from spectroscopic trace gas measurements in the tropical mid-stratosphere

L. Kritten<sup>1,\*</sup>, A. Butz<sup>2,\*</sup>, M. P. Chipperfield<sup>3</sup>, M. Dorf<sup>4,\*</sup>, S. Dhomse<sup>3</sup>, R. Hossaini<sup>3</sup>, H. Oelhaf<sup>2</sup>, C. Prados-Roman<sup>5,\*</sup>, G. Wetzel<sup>2</sup>, and K. Pfeilsticker<sup>6</sup>

<sup>1</sup>Institute for Space Sciences (WEW), Free University Berlin, Berlin, Germany

<sup>2</sup>Karlsruhe Institute of Technology, IMK-ASF, Karlsruhe, Germany

<sup>3</sup>Institute for Climate and Atmospheric Science, School of Earth and Environment, University of Leeds, Leeds, UK

<sup>4</sup>Max-Planck-Institute for Chemistry, Mainz, Germany

<sup>5</sup>Atmospheric Chemistry and Climate Group, Institute of Physical Chemistry Rocasolano (CSIC), Madrid, Spain

<sup>6</sup>Institute of Environmental Physics (IUP), University of Heidelberg, Heidelberg, Germany

\*formerly at: Institute of Environmental Physics (IUP), University of Heidelberg, Heidelberg, Germany

Title Page

Abstract

Introduction

Conclusions

References

Tables

Figures

◀

▶

◀

▶

Back

Close

Full Screen / Esc

Printer-friendly Version

Interactive Discussion



Received: 18 November 2013 – Accepted: 2 February 2014 – Published: 20 February 2014

Correspondence to: L. Kritten (lkritten@wew.fu-berlin.de)

Published by Copernicus Publications on behalf of the European Geosciences Union.

ACPD

14, 4687–4721, 2014

## Stratospheric limb measurements

L. Kritten et al.

Title Page

Abstract

Introduction

Conclusions

References

Tables

Figures

◀

▶

◀

▶

Back

Close

Full Screen / Esc

Printer-friendly Version

Interactive Discussion



## Abstract

The absorption cross-section of  $\text{N}_2\text{O}_5$ ,  $\sigma_{\text{N}_2\text{O}_5}(\lambda, T)$ , which is known from laboratory measurements with the uncertainty of a factor of 2 (Table 4-2 in JPL-2011, Sander et al., 2011), was investigated by balloon-borne observations of the relevant trace gases in the tropical mid-stratosphere. The method relies on the observation of the diurnal variation of  $\text{NO}_2$  supported by detailed photochemical modelling of  $\text{NO}_y$  ( $\text{NO}_x (= \text{NO} + \text{NO}_2) + \text{NO}_3 + 2\text{N}_2\text{O}_5 + \text{ClONO}_2 + \text{HO}_2\text{NO}_2 + \text{BrONO}_2 + \text{HNO}_3$ ) photochemistry. Simulations are initialised with  $\text{O}_3$  measured by direct sun observations, the  $\text{NO}_y$  partitioning from MIPAS-B (Michelson Interferometer for Passive Atmospheric Sounding-Balloon) observations in similar air masses at nighttime, and all other relevant species from simulations of the SLIMCAT chemical transport model (CTM). Best agreement between the simulated and observed diurnal increase of  $\text{NO}_2$  is found if the  $\sigma_{\text{N}_2\text{O}_5}(\lambda, T)$  is scaled by a factor of  $1.6 \pm 0.8$  in the UV-C (200–260 nm) and by a factor of  $0.9 \pm 0.26$  in the UV-B/A (260–350 nm), compared to current recommendations. In consequence, at 30 km altitude, the  $\text{N}_2\text{O}_5$  lifetime against photolysis becomes a factor of 0.77 shorter at solar zenith angle (SZA) of  $30^\circ$  than using the recommended  $\sigma_{\text{N}_2\text{O}_5}(\lambda, T)$ , and stays more or less constant at SZAs of  $60^\circ$ . Our scaled  $\text{N}_2\text{O}_5$  photolysis frequency slightly reduces the lifetime (0.2–0.6 %) of ozone in the tropical mid- and upper stratosphere, but not to an extent to be important for global ozone.

## 1 Introduction

The  $\text{NO}_x$  ozone loss cycle dominates catalytic ozone loss in the mid-stratosphere (25–45 km). In future it is predicted to increase further in relevance, since the emissions of its major precursor  $\text{N}_2\text{O}$  are increasing, while emissions of other ozone-depleting substances (ODS) are decreasing (Ravishankara et al., 2009). Signs that this is already happening come from the recent analysis of ozone vertical profile time series from SCIAMACHY satellite instrument limb measurements (Gebhardt et al., 2013), since

## Stratospheric limb measurements

L. Kritten et al.

Title Page

Abstract

Introduction

Conclusions

References

Tables

Figures

◀

▶

◀

▶

Back

Close

Full Screen / Esc

Printer-friendly Version

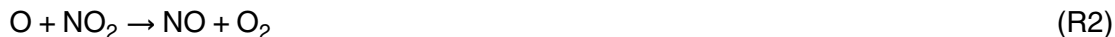
Interactive Discussion



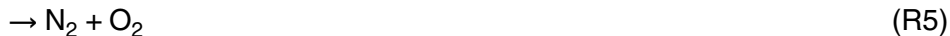
they show a negative trend of ozone in the tropics above 30 km and a positive trend below. The explanation most favoured by the authors is due to  $\text{NO}_x$  photochemistry, which catalytically destroys stratospheric ozone (e.g., Crutzen, 1970; Johnston, 1971) (see below).

5 A second motivation to study the photolysis frequency of  $\text{N}_2\text{O}_5$  comes through the finding of often overpredicted  $\text{N}_2\text{O}_5$ , most strikingly found in comparison studies of MIPAS/ENVISAT  $\text{N}_2\text{O}_5$  data with predictions of a suite of photochemical transport models for the lower and middle stratosphere ( $p > 10$  mbar) at (e.g., Brühl et al., 2007; Funke et al., 2011). Unpublished SLIMCAT sensitivity runs are indicating that a more rapid  
10 photolysis of  $\text{N}_2\text{O}_5$  (up to factor of 2) than supported by  $\sigma_{\text{N}_2\text{O}_5}(\lambda, T)$  from JPL-2011 (Sander et al., 2011) would largely help to close this gap.

In the context of ozone loss, most crucial is how fast major nighttime  $\text{NO}_y$  species (e.g.,  $\text{HNO}_3$ ,  $\text{N}_2\text{O}_5$ , and  $\text{ClONO}_2$ ) are recycled into ozone destroying  $\text{NO}_x$  at daytime. Catalytic ozone destruction by the  $\text{NO}_x$  photochemistry occurs through the following  
15 reactions



The primary source of stratospheric  $\text{NO}_x$  is the photolytic destruction of  $\text{N}_2\text{O}$  (Reactions  
20 R4–R6).



$\text{N}_2\text{O}$  is mostly emitted by biological and combustion processes at the surface, but  
25 their  $\text{N}_2\text{O}$  emissions are not regulated by the Montreal Protocol (e.g., IPCC, 2007; WMO, 2011). Accordingly, atmospheric  $\text{N}_2\text{O}$  concentrations are presently increasing with a rate of 0.75 ppb per year (Park et al., 2012 and WMO Press Release, 2014).

## Stratospheric limb measurements

L. Kritten et al.

Title Page

Abstract

Introduction

Conclusions

References

Tables

Figures

◀

▶

◀

▶

Back

Close

Full Screen / Esc

Printer-friendly Version

Interactive Discussion



Stratospheric limb  
measurements

L. Kritten et al.

Title Page

Abstract

Introduction

Conclusions

References

Tables

Figures

◀

▶

◀

▶

Back

Close

Full Screen / Esc

Printer-friendly Version

Interactive Discussion



Four major processes determine the effect of  $\text{N}_2\text{O}$  on stratospheric ozone:

(1) The competition of the  $\text{N}_2\text{O}$  destruction processes (Reaction R4) leading to  $\text{NO}_x$  production (about 7 % for any  $\text{N}_2\text{O}$  destroyed) and Reactions (R5) and (R6) only destroying  $\text{N}_2\text{O}$  without producing  $\text{NO}_x$ .

(2) The sink Reactions (R7) and (R8)



followed by



are known to destroy  $\text{NO}_x$  in the middle and upper stratosphere.

(3) Further it is well known that during daytime Reaction (R1) and the photolysis of  $\text{NO}_2$



readily establish a steady state between  $\text{NO}$  and  $\text{NO}_2$ , thus determining the amount of  $\text{NO}_2$  available for the odd-oxygen-destroying Reaction (R2).

(4) The fourth major factor controlling the ozone depletion potential of  $\text{NO}_x$ , and thus of  $\text{N}_2\text{O}$ , are reactions leading to the so-called  $\text{NO}_y$  reservoir species ( $\text{NO}_y = \text{NO}_x + \text{NO}_3 + 2\text{N}_2\text{O}_5 + \text{ClONO}_2 + \text{HO}_2\text{NO}_2 + \text{BrONO}_2 + \text{HNO}_3$ ) of which all except  $\text{HNO}_3$  are important for the diurnal variation of  $\text{NO}_x$ , and thus  $\text{NO}_x$ -mediated ozone loss. Among them  $\text{N}_2\text{O}_5$  is most important in the tropical mid-stratosphere (as shown in Fig. 1). First  $\text{NO}_3$  has to be formed by the reaction



then  $\text{N}_2\text{O}_5$  can be formed by the termolecular reaction



and destroyed by thermal decomposition (Reaction R12), photolysis (Reaction R13), and the heterogeneous Reaction (R14), where aerosols are abundant, i.e. in the lower stratosphere (Brasseur and Solomon, 2005).



Reaction (R13) is particularly relevant for the daytime increase of  $\text{NO}_x$  in the tropical mid-stratosphere, since the product of photolysis rate  $J_{\text{N}_2\text{O}_5}$  and concentration of  $\text{N}_2\text{O}_5$  is the largest among the reservoir species under the given conditions (see Fig. 1). The  $J_{\text{N}_2\text{O}_5}$  is determined by the actinic flux  $F(\lambda)$ , the quantum yield for photo-dissociation  $\phi(\lambda)$  and the absorption cross-section of  $J_{\text{N}_2\text{O}_5}$ ,  $\sigma_{\text{N}_2\text{O}_5}(\lambda, T)$  (Brasseur and Solomon, 2005), leading to the photolysis rate  $J_{\text{N}_2\text{O}_5}$

$$10 \quad J_{\text{N}_2\text{O}_5} = \int F(\lambda, \text{SZA}) \cdot \sigma_{\text{N}_2\text{O}_5}(\lambda, T) \cdot \phi(\lambda) \cdot d\lambda \quad (1)$$

The slightly temperature-dependent  $\sigma_{\text{N}_2\text{O}_5}(\lambda, T)$  decreases from the extreme UV-C ( $\lambda = 200 \text{ nm}$ ) to the visible spectral range ( $\lambda = 400 \text{ nm}$ ) over 8 to 9 orders of magnitude (Fig. 2). On the other hand the actinic flux  $F(\lambda)$  strongly increases with wavelength resulting in two distinct maxima of the actinic spectrum in the mid- and upper stratosphere (i.e. in the UV-C and UV-B) (Fig. 3), of which the shape depends on the solar zenith angle (SZA). The short wavelength maximum of the actinic spectrum is located around  $\lambda = 220 \text{ nm}$  and the long wavelength maximum between  $\lambda = 280$  and  $320 \text{ nm}$ .

In the laboratory,  $\sigma_{\text{N}_2\text{O}_5}(\lambda, T)$  was first measured by Jones and Wulf (1937) and later by many others (see Sect. 2.2). Current estimates of  $\sigma_{\text{N}_2\text{O}_5}(\lambda, T)$  together with its uncertainties (a factor of 2) are reported in the JPL-2011 compendium (Table 4-2). However, to our knowledge  $\sigma_{\text{N}_2\text{O}_5}(\lambda, T)$  has never been inferred from field observations.

25 Here balloon-borne measurements in the tropical mid-stratosphere of the diurnal variation of  $\text{NO}_2$  (Kritten et al., 2010) are exploited to infer  $\sigma_{\text{N}_2\text{O}_5}(\lambda, T)$  under

Stratospheric limb measurements

L. Kritten et al.

Title Page

Abstract

Introduction

Conclusions

References

Tables

Figures

◀

▶

◀

▶

Back

Close

Full Screen / Esc

Printer-friendly Version

Interactive Discussion



## Stratospheric limb measurements

L. Kritten et al.

Title Page

Abstract

Introduction

Conclusions

References

Tables

Figures

◀

▶

◀

▶

Back

Close

Full Screen / Esc

Printer-friendly Version

Interactive Discussion



stratospheric conditions. For the interpretation of the measured data with respect to  $\sigma_{\text{N}_2\text{O}_5}(\lambda, T)$ , a 1-D photochemical model is used. The model is initialised and further constrained by trace gas observations ( $\text{O}_3$ , and a suite of  $\text{NO}_y$  species) taken within the so-called tropical pipe over north-eastern Brazil during summer 2005. Further, an optimal estimation approach is used to minimise the quadratic difference of the measured from modelled concentration field of  $\text{NO}_2$  as a function of time and height. For this purpose  $\sigma_{\text{N}_2\text{O}_5}(\lambda, T)$  is scaled by two free parameters (denoted by  $s_1$  and  $s_2$ ) in the extreme UV-C (200–258 nm) (denoted by  $w_1$  wavelength range), and UV-B/A spectral range (260–420 nm) (denoted by  $w_2$  wavelength range), respectively.

The paper is organised as follows. In Sect. 2 the tools used in the study are described, including the  $\text{NO}_2$  measurements, some details of the  $\text{NO}_y$  photochemical modelling as well as the mathematics to retrieve  $\sigma_{\text{N}_2\text{O}_5}(\lambda, T)$ . Section 3 reports on the results and discusses uncertainties. Section 4 addresses the implication of our findings for stratospheric  $\text{N}_2\text{O}_5$  and global ozone. Section 5 concludes the study.

## 2 Measurements, photochemical modelling, and $\sigma_{\text{N}_2\text{O}_5}(\lambda, T)$ retrieval

This section describes our approach to constrain  $\sigma_{\text{N}_2\text{O}_5}(\lambda, T)$  from the  $\text{NO}_2$  measurements in the tropical mid-stratosphere (Kritten et al., 2010) (Sect. 2.1). Further the photochemical modelling including its initialisation by information gained from additional trace gas measurements in the tropical stratosphere and from simulations of the SLIMCAT CTM (Sect. 2.2) is described. Finally the retrieval of the scaling parameters of  $\sigma_{\text{N}_2\text{O}_5}(\lambda, T)$  for two wavelength intervals  $w_1$  and  $w_2$  (Sect. 2.3) are discussed.

### 2.1 Measurements

For this study, time-dependent profiles of stratospheric  $\text{NO}_2$  are used, which were measured over north-eastern Brazil (5.1° S, 43.6° W) on 30 June 2005 (see Fig. 8 in Kritten et al., 2010). During the balloon flight 187 limb spectra were recorded during 17 limb

**Stratospheric limb measurements**

L. Kritten et al.

Title Page

Abstract

Introduction

Conclusions

References

Tables

Figures

◀

▶

◀

▶

Back

Close

Full Screen / Esc

Printer-friendly Version

Interactive Discussion



sequences, which covers 5:35 h from local sunrise (07:30 LT) into the early afternoon (13:05 LT). The measured limb spectra were analyzed for differential slant column densities (DSCDs) using the DOAS (Differential Optical Absorption Spectroscopy) technique (e.g., Weidner et al., 2005; Platt and Stutz, 2008). Prior to the inversion of the measured DSCDs into a NO<sub>2</sub> concentration height and time field, the radiative transfer for each measurement is modelled using the radiative transfer model (RTM) McArtim (Deutschmann et al., 2011). Further, the RT calculations are validated against measured limb radiances and inferred O<sub>4</sub> and O<sub>3</sub>. The measured array of NO<sub>2</sub> DSCDs is then projected into a NO<sub>2</sub> concentration vs. height and time field of equal altitude ( $h_i = 0.5$  km) and time spacing ( $t_j = 30$  min), using the optimal estimation technique (e.g., Rodgers, 2000; Kritten et al., 2010). Due to decay of the NO<sub>y</sub> reservoir species during daytime, at 33 km where the NO<sub>2</sub> profile peaks, NO<sub>2</sub> increases by roughly 60 % during our observation. Our analysis is limited to SZAs  $\leq 85^\circ$  in order to reduce effects due to refraction which is not properly accounted for in the RTM McArtim (Deutschmann et al., 2011).

Major errors and shortcomings of our NO<sub>2</sub> measurements are the remaining pitch and azimuth angle oscillations of the balloon platform (see Fig. 6 in Kritten et al., 2010). While the former lead to a vertical jitter in the field of view, resulting in an up to  $\pm 10\%$  uncertainty in the inferred NO<sub>2</sub> concentrations, the azimuth angle oscillations are more difficult to deal with. The latter is mainly due to the importance of polarisation (which is not yet considered in our RTM) of the scattered light from stratospheric limb measurements in the UV/visible wavelength range, mainly if during the course of the measurements the azimuthal scattering angle changes. Therefore, in order to remove any systematic errors due to the movement of the balloon gondola, the inferred NO<sub>2</sub> field is re-normalised using the inferred field of O<sub>3</sub>. This is justified, by the constant O<sub>3</sub> concentration during the course of the measurement, and the similar optical depths at the wavelengths considered in the spectral analysis of O<sub>3</sub> and NO<sub>2</sub>. For this purpose a weighting matrix is derived by dividing the retrieved O<sub>3</sub> concentration for each altitude

( $h_i$ ) and time ( $t_j$ ) step by the mean  $O_3$  concentration of the whole balloon flight.

$$[NO_{2,corr}]_{i,j} = [NO_{2,retr}]_{i,j} \cdot \frac{[O_{3,mean}]_{i,j}}{[O_{3,retr}]_{i,j}} \quad (2)$$

It is found that the re-normalisation alters the  $NO_2$  field by 15% at most. Further on in the study, the renormalised  $NO_2$  field (shown in the lower panel of Fig. 4) is used, rather than the field inferred in Kritten et al. (2010) (see Fig. 8 therein).

## 2.2 Modelling of the $NO_y$ photochemical system

Since for the present study the calculation of the photolysis rates and the photochemical evolution is crucial, both deserve to be addressed. The photolysis rates are calculated by a module adopted from the SLIMCAT 3-D CTM (Bösch et al., 2003; Chipperfield, 2006) with updated molecular absorption cross-sections for  $N_2O_5$  and  $HNO_3$  (Sander et al., 2011). First, the actinic fluxes are calculated as recommended by Lary and Pyle (1991) and stored in a look-up table. Then, in order to scale the actinic fluxes to the actual atmospheric conditions, the calculated photolysis rates are interpolated to the actual pressure, temperature, SZA, and overhead ozone. For the latter an ozone profile measured by balloon-borne solar occultation observations a few days prior to the  $NO_2$  measurements is used (Butz et al., 2006).  $J_{N_2O_5}$  skylight radiances were already validated in previous studies of our group (e.g., Bösch et al., 2003; Deutschmann et al., 2011).

For calculation of  $J_{N_2O_5}$ , the  $\sigma_{N_2O_5}(\lambda, T)$  based on the recommendation of the JPL-2011 compendium as shown in Fig. 2) is used (Sander et al., 2011).  $\sigma_{N_2O_5}(\lambda, T)$  ranges over about 9 orders of magnitude (from about  $10^{-17} \text{ cm}^2$  at 200 nm to  $10^{-26} \text{ cm}^2$  at 450 nm). The temperature dependence of  $\sigma_{N_2O_5}(\lambda, T)$  is derived according to Harwood et al. (1993). This only becomes significant at wavelengths larger 280 nm, where  $\sigma_{N_2O_5}(\lambda, T)$  decreases (decreasing temperature with an increasing T-dependence for larger wavelengths).

Title Page

Abstract

Introduction

Conclusions

References

Tables

Figures

◀

▶

◀

▶

Back

Close

Full Screen / Esc

Printer-friendly Version

Interactive Discussion



Stratospheric limb  
measurements

L. Kritten et al.

Title Page

Abstract

Introduction

Conclusions

References

Tables

Figures

◀

▶

◀

▶

Back

Close

Full Screen / Esc

Printer-friendly Version

Interactive Discussion



The study of Oh et al. (1986) indicates that, besides  $\text{NO}_3$ , the primary photolysis products of  $\text{N}_2\text{O}_5$  are a wavelength-dependent mixture of  $\text{NO}_2$ ,  $\text{NO}_2^*$  and  $\text{NO}+\text{O}$ , where  $\text{NO}_2^*$  represents  $\text{NO}_2$  in an excited electronic state. The measured quantum yield for the  $\text{NO}_3$  production is close to unity. The combined uncertainties of the absorption cross-section and quantum yield cause  $\sigma_{\text{N}_2\text{O}_5}$  to be uncertain by a factor of 2.

Figure 3 displays the actinic spectrum relevant for the photolysis of  $\text{N}_2\text{O}_5$  at stratospheric conditions. It shows that two distinct wavelength regions are important for the photolysis of  $\text{N}_2\text{O}_5$ . In the wavelength region  $w_1$  (200–258 nm) where  $\sigma_{\text{N}_2\text{O}_5}(\lambda, T)$  increases strongly, the combined effects of the  $\text{O}_3$  absorption in the Hartley band, and the  $\text{O}_2$  absorption in the Schumann-Runge band ( $< 242$  nm), lead to a strong attenuation of the actinic flux in the mid-stratosphere and therefore to a decrease in the actinic spectrum. Thus, overhead  $\text{O}_2$  and  $\text{O}_3$  are crucial for the photolysis of  $\text{N}_2\text{O}_5$  in the UV-C. In the wavelength region  $w_2$  (260–420 nm), the strongly increasing actinic flux and the decreasing absorption of  $\text{O}_3$  competes with the strong decrease in  $\sigma_{\text{N}_2\text{O}_5}(\lambda, T)$  with wavelength, leading to a second maximum of the actinic spectrum for  $\text{N}_2\text{O}_5$  photolysis. The relative importance of each maximum depends on altitude and SZA. Therefore, if overhead ozone and total air mass is held fixed, observations at different altitudes and SZAs may provide independent information on the contribution of each wavelength region to  $J_{\text{N}_2\text{O}_5}$ . Noteworthy is also that in the wavelength range  $w_1$ ,  $\sigma_{\text{N}_2\text{O}_5}(\lambda, T)$  is temperature-independent and in  $w_2$  temperature-dependent (Fig. 2).

The temporal evolution of the  $\text{NO}_y$  species is modelled on 11 height levels (located between 655 K potential temperature (25.5 km) and 1099 K (35.5 km)) using the 1-D chemistry model LABMOS, which is an updated version of the model used by Bösch et al. (2003). It includes all relevant photochemical reactions of oxygen, nitrogen, hydrogen, chlorine, and bromine species according to kinetic and thermochemical data compiled in Sander et al. (2011). The model was integrated for 10 days using the commercial Facsimile software. All modelled data shown are taken from the 10th day of the respective model run, in order to allow for spin-up of the  $\text{NO}_y$  partitioning.

## Stratospheric limb measurements

L. Kritten et al.

Title Page

Abstract

Introduction

Conclusions

References

Tables

Figures

◀

▶

◀

▶

Back

Close

Full Screen / Esc

Printer-friendly Version

Interactive Discussion



The model is initialised for most species using the output of SLIMCAT simulations (Chipperfield, 2006) (run-id 336) for 5° N, 43° E for 02:00 LT on 17 June 2005, except for NO<sub>y</sub> species, O<sub>3</sub> and NO<sub>2</sub>. For initialisation of the NO<sub>y</sub> species (i.e., HNO<sub>3</sub>, N<sub>2</sub>O<sub>5</sub>, ClONO<sub>2</sub>, HO<sub>2</sub>NO<sub>2</sub>, and BrONO<sub>2</sub>), the measurements of the MIPAS-B (Michelson Interferometer for Passive Atmospheric Sounding-Balloon) instrument are taken, which were recorded 17 days prior to the mini-DOAS NO<sub>2</sub> measurements (e.g., Wetzela et al., 2002, and unpublished data). The model is further constrained by ozone measured by solar occultation measurements taken from the LPMA/DOAS payload (Limb Profile Monitor of the Atmosphere/Differential Optical Absorption Spectroscopy) 13 days prior to the NO<sub>2</sub> measurements.

Small mismatches in measured and modelled total NO<sub>y</sub> are again removed by re-normalisation with the factor ( $\widehat{\text{NO}}_y$ ) of the concentrations (NO<sub>y</sub>, *i*) of the different NO<sub>y</sub> species (Wiegele et al., 2009):

$$\widehat{\text{NO}}_y = \text{NO}_{y, \text{MIPAS-B}} / \text{NO}_{y, \text{SLIMCAT}}, \quad (3)$$

such that the NO<sub>y</sub> partitioning given by SLIMCAT is preserved, but the total amount is constrained to the NO<sub>y</sub> measured by the MIPAS-B instrument. Depending on the altitude, the normalisation factor ranges between 1 and 1.2. Figure 1 provides an overview on how the different NO<sub>y</sub> species contribute to daytime NO<sub>x</sub> production at different altitudes. Here the lower boundary of the striped area denotes the temporal evolution of the particular gas, and the striped area shows the total amount of NO<sub>x</sub>, which is released by photolysis from the considered NO<sub>y</sub> species. The dominant role of N<sub>2</sub>O<sub>5</sub> destruction (red) for NO<sub>x</sub> formation by Reactions (R11), and Reaction (R12) in the tropical mid-stratosphere at daytime is evident. In contrast all the other NO<sub>y</sub> species including HNO<sub>3</sub> destruction contribute to less than 10% to the NO<sub>x</sub> increase during daytime.

## 2.3 Retrieval of $\sigma_{\text{N}_2\text{O}_5}(\lambda, T)$

If the model was complete (i.e. there was no missing chemistry), a comparison of measurements and model should provide information about the accuracy of the model and its components. We refer to the model output as  $\text{NO}_{2\text{calc}}$ , and the measured  $\text{NO}_2$  as  $\text{NO}_{2\text{meas}}$ . However, “calculated” concentrations are not totally independent from the measurements, since  $\text{O}_3$  is relevant for the calculation of the actinic fluxes (see Sect. 2.2) and the partitioning of  $\text{NO}_y$  contributes to  $\text{NO}_{2\text{calc}}$ . Figure 4 shows  $\text{NO}_{2\text{calc}}$  and  $\text{NO}_{2\text{meas}}$  in the upper and lower panel, respectively. In the following we describe how the parameters  $s_1$  and  $s_2$  are retrieved from the measured and modelled field of  $\text{NO}_2$ . They are defined by

$$s_1 \cdot \sigma_{\text{N}_2\text{O}_5}(200\text{--}258 \text{ nm})_{\text{lab}} = \sigma_{\text{N}_2\text{O}_5}(200\text{--}258 \text{ nm})_{\text{ret}} \quad (4)$$

$$s_2 \cdot \sigma_{\text{N}_2\text{O}_5}(260\text{--}350 \text{ nm})_{\text{lab}} = \sigma_{\text{N}_2\text{O}_5}(260\text{--}350 \text{ nm})_{\text{ret}} \quad (5)$$

where the subscripts lab and ret and denote the laboratory measured and retrieved  $\sigma_{\text{N}_2\text{O}_5}$ , respectively. The measurement vector  $\mathbf{y}$  is given by the subsequently measured  $\text{NO}_2$  concentrations for  $h_i$  and  $t_j$  (Sect. 2.1)

$$y_{i,j} = \text{NO}_2(h_i, t_j) \quad (6)$$

and the state  $\mathbf{x}$  is defined by the scaling factors  $s_1$  and  $s_2$ .

$$x_k = s_k \quad (7)$$

The sensitivity of the  $\text{NO}_2$  field to  $s_1$  and  $s_2$  can be quantitatively expressed by a weighting function or Jacobian matrix of derivatives of  $[\text{NO}_2]_{i,j}$  with respect to the parameters  $s_1$  and  $s_2$ , i.e.,  $\partial[\text{NO}_2]_{i,j}/\partial s_k$ . For a given  $\text{NO}_2$  profile with the indices  $i$  for a given altitude  $h_i$  and  $j$  for a given time  $t_j$  (Fig. 5), the Jacobian with respect to  $s_1$  and  $s_2$  reads

$$K_{i,j,k} = \frac{\partial y_{i,j}}{\partial x_k} \quad (8)$$

Title Page

Abstract

Introduction

Conclusions

References

Tables

Figures

◀

▶

◀

▶

Back

Close

Full Screen / Esc

Printer-friendly Version

Interactive Discussion



The forward model  $F(x) = \mathbf{y}$  is constructed from the photochemical model as described in Sect. 2.2

The inferred sensitivity (i.e., Jacobians  $K_{i,j,k}$ ) for  $s_1$  and  $s_2$  is shown in Fig. 5. For  $s_1$  it is a factor of 6 lower than for  $s_2$ , but both peak around 28 to 35 km altitude, i.e., where the measurements are taken. The maximum sensitivity ( $\partial[\text{NO}_2]_{i,j}/\partial s_k$ ) is more extended in time for  $s_2$  than for  $s_1$ , since in the UV-C ( $w_1$ ) the spectral actinic flux is more dependent on SZA as compared to the UV-B/A wavelength range ( $w_2$ ). Furthermore  $\partial[\text{NO}_2]_{i,j}/\partial s_1$  peaks at higher altitudes as compared to  $\partial[\text{NO}_2]_{i,j}/\partial s_2$ , since attenuation in the UV-C occurs at smaller overhead air masses as compared to the UV-B/A wavelength range. For the purpose of a retrieval of  $s_1$  and  $s_2$  the vector  $y_{i,j}$  is transformed into a 1-dimensional vector  $\mathbf{y}$ , that contains the  $\text{NO}_2$  profiles for subsequent time steps  $t_j$ . Similarly, the kernel  $K_{i,j,k}$  is transformed into a 2-dimensional matrix  $\mathbf{K}$ . In order to provide enough information on the state and to make the inversion mathematically feasible we need an additional constraint. Since an a priori  $\mathbf{x}_a$  (first guess) and a priori covariance (it's error matrix) is available and well defined, namely  $\sigma_{\text{N}_2\text{O}_5}$  from laboratory measurements and their inherent error, we chose the optimal estimation technique (Rodgers, 2000) to estimate  $s_1$  and  $s_2$ . Here, the retrieved state  $\hat{\mathbf{x}}$  is constructed from both, prior information and the measurements, each weighted by the covariances  $\mathbf{S}_a$  and  $\mathbf{S}_e$ , respectively. The relationship between measurement and state is examined by the cost function defined by

$$\chi^2 = (\hat{\mathbf{x}} - \mathbf{x}_a)\mathbf{S}_a^{-1}(\hat{\mathbf{x}} - \mathbf{x}_a)^T + (\mathbf{y}_{\text{mod}} - \mathbf{y}_{\text{meas}})\mathbf{S}_e^{-1}(\mathbf{y}_{\text{mod}} - \mathbf{y}_{\text{meas}})^T \quad (9)$$

Since the measurement and the state do not linearly map, the state  $\mathbf{x}$  is iteratively retrieved from (the subscript  $i$  now denotes the  $i$ th step)

$$\hat{\mathbf{x}}_{i+1} = \mathbf{x}_i + \left(\mathbf{S}_a^{-1} + \mathbf{K}_i^T \mathbf{S}_e^{-1} \mathbf{K}_i\right)^{-1} \cdot \left[\mathbf{K}_i^T \mathbf{S}_e^{-1} (\mathbf{y} - F(\mathbf{x}_i)) - \mathbf{S}_a^{-1}(\mathbf{x}_i - \mathbf{x}_a)\right] \quad (10)$$

where  $\mathbf{K}_i$  is derived before each iteration for the current state  $\mathbf{x}_i$ . As the starting state we choose  $\mathbf{x}_0 = \mathbf{x}_a$ . The diagonal elements of the measurement covariance  $\mathbf{S}_e$  represent

## Stratospheric limb measurements

L. Kritten et al.

Title Page

Abstract

Introduction

Conclusions

References

Tables

Figures

◀

▶

◀

▶

Back

Close

Full Screen / Esc

Printer-friendly Version

Interactive Discussion



the squared error of the retrieved NO<sub>2</sub> measurements, whereas the diagonal elements of  $\mathbf{S}_a$  are filled with the squared error of the laboratory measurements. For convergence criteria a certain step size from iteration  $i$  to  $i + 1$  is defined (Rodgers, 2000)

$$\sqrt{(x_{i+1} - x_i)^2} \leq 0.04, \quad (11)$$

which is about one order of magnitude smaller than the expected noise error of the solution, as derived in Sect. 3.1.

### 3 Results and Discussion

Figure 6 shows  $\chi^2$  in the parameter space  $s_1$  and  $s_2$ , where the minimum region ( $\chi^2 = 30$ ) is located at around  $s_1 = 1.2$  to  $2.6$  and  $s_2 = 0.7$  to  $1.1$ . After 10 iterations the global minimum is found at  $s_1 = 1.6$  and  $s_2 = 0.9$ , i.e. our retrieval indicates a  $\sigma_{\text{N}_2\text{O}_5}(\lambda, T)$  a factor 1.6 larger in the UV-C spectral range and a factor 0.9 smaller in the UV-B/A spectral range as compared to the recommended value in JPL-2011, with retrieval uncertainties of  $\pm 0.80$  and  $\pm 0.26$  for  $s_1$  and  $s_2$ , respectively (see next section). Figure 6 shows the inferred result in the  $s_2/s_1$  space together with their uncertainties, and the recommended JPL-2011 values. Figure 7 shows the resulting  $\sigma_{\text{N}_2\text{O}_5}$ .

Figure 4 shows the modelled (unscaled  $s_1$  and  $s_2$  in the upper panel, scaled  $s_1$  and  $s_2$  in the middle panel) and the measured diurnal NO<sub>2</sub> concentration (lower panel). Since there is still some discrepancy in the diurnal behaviour of the forward modelled state and the measurement, in the next section we investigate to what extent the errors and uncertainties of the measurement, as well as errors and uncertainties of the forward model, propagate into the inferred  $s_1$  and  $s_2$  values (see Table 1 for an overview on the errors and uncertainties).

Title Page

Abstract

Introduction

Conclusions

References

Tables

Figures

◀

▶

◀

▶

Back

Close

Full Screen / Esc

Printer-friendly Version

Interactive Discussion



### 3.1 Retrieval uncertainties

The measurement error ( $\mathbf{S}_{\text{noise}}$ ) of  $\text{NO}_2$  has already been discussed by Kritten et al. (2010). According to Rodgers (2000), the propagation of the measurement noise into the retrieval noise can be quantified by

$$5 \quad \mathbf{S}_{\text{noise}} = \left( \mathbf{K}^T \mathbf{S}_e^{-1} \mathbf{K} \right)^{-1}. \quad (12)$$

which leads to  $1 - \sigma$  errors of  $\pm 0.80$  and  $\pm 0.26$  for  $s_1$  and  $s_2$ , respectively.

### 3.2 Uncertainties in the forward model

We now discuss errors and uncertainties of  $s_1$  and  $s_2$  due to uncertainties in the forward model parameters, which are input parameters that influence the state but are not retrieved (Rodgers, 2000). Since the model is not linear in the forward model parameters, additional local retrievals of  $s_1$  and  $s_2$  at both the lower and upper boundary of the uncertainty range of these parameters are required. The difference in the retrieved  $s_1$  and  $s_2$  compared to the undisturbed case is taken as a measure for the uncertainty. The uncertainties are not symmetrical, hence in each case an upper and a lower range of uncertainty is given. The forward model parameters in this study are input parameters to the chemical model. Among the many input parameters (i.e. model initialisation parameters as well as kinetic and thermochemical data), only those parameters which arguably exert the most influence on the results are considered. For model initialisation, these are total  $\text{NO}_y$  and  $\text{O}_3$ , and the absorption cross-section of  $\text{NO}_2$ . We also discuss the uncertainty in the actinic flux going into the calculation of  $J_{\text{N}_2\text{O}_5}$ . The following results are obtained:

(1) Initialisation of  $\text{NO}_y$ : as outlined above (Sect. 2.2), the total amount of  $\text{NO}_y$  is initialised from MIPAS-B measurements. The accuracy of the MIPAS-B  $\text{NO}_y$  measurements above 20 km ranges between 4 and 7 %. When initialising the model with  $\text{NO}_y$  at the lower boundary of the uncertainty range, the retrieval gives  $s_1 = 2.1$  and  $s_2 = 1.0$ .

When initialising the model with  $\text{NO}_y$  at the upper boundary of the uncertainty range, the retrieval gives  $s_1 = 1.3$  and  $s_2 = 0.7$ . Accordingly the uncertainties due to initialisation of  $\text{NO}_y$  are  $\Delta s_1 = +0.5 / -0.3$  and  $\Delta s_2 = +0.1 / -0.2$ .

(2) Initialisation of  $\text{O}_3$ : as outlined above (Sect. 2.2), the  $\text{O}_3$  profile is initialised from direct sun DOAS observations. The accuracy of these measurements above 20 km ranges between 5 and 29 %. When initialising the model with  $\text{O}_3$  at the lower boundary of the uncertainty range, the retrieval gives  $s_1 = 1.3$  and  $s_2 = 0.7$ . When initialising the model with  $\text{O}_3$  at the upper boundary of the uncertainty range, the retrieval gives  $s_1 = 1.9$  and  $s_2 = 1.2$ . Accordingly, the uncertainties due to initialisation of  $\text{O}_3$  are  $\Delta s_1 = +0.3 / -0.4$  and  $\Delta s_2 = +0.3 / -0.2$ .

(3) Absorption cross-section of  $\text{NO}_2$  (see Reaction R9): the combined uncertainty of the  $\text{NO}_2$  absorption cross-section and the quantum yield is a factor of 1.2 (Sander et al., 2011). When calculating the photolysis rates of  $\text{NO}_2$  at the lower boundary of the uncertainty range of  $\sigma_{\text{N}_2\text{O}_5}(\lambda, T)$ , the retrieval gives  $s_1 = 1.1$  and  $s_2 = 0.6$ . When calculating the photolysis rates of  $\text{NO}_2$  at the upper boundary of the uncertainty range of  $\sigma_{\text{NO}_2}(\lambda, T)$ , the retrieval gives  $s_1 = 2.2$  and  $s_2 = 1.2$ . Accordingly the uncertainties due to  $\sigma_{\text{NO}_2}(\lambda, T)$  are  $\Delta s_1 = +0.6 / -0.6$  and  $\Delta s_2 = +0.3 / -0.3$ . Evidently, despite its relatively small uncertainty, uncertainties in  $\sigma_{\text{NO}_2}(\lambda, T)$  directly propagate into the modelled  $\text{NO}_2$  concentration.

(4) The rate constant  $k_{\text{NO}+\text{O}_3}$  (see Reaction R1): the uncertainty of the rate constant  $k_{\text{NO}+\text{O}_3}$  is temperature-dependent (Sander et al., 2011) and varies at temperatures relevant for this study between a factor of 1.30 and 1.42. When implementing a rate constant  $k_{\text{NO}+\text{O}_3}$  at the lower boundary of the uncertainty range, the retrieval gives  $s_1 = 2.1$  and  $s_2 = 1.5$ . When implementing a rate constant  $k_{\text{NO}+\text{O}_3}$  at the upper boundary of the uncertainty range, the retrieval gives  $s_1 = 0.7$  and  $s_2 = 0.6$ . Accordingly, the uncertainties due to the rate constant  $k_{\text{NO}+\text{O}_3}$  are  $\Delta s_1 = +0.5 / -0.9$  and  $\Delta s_2 = +0.6 / -0.3$ .

(5) Actinic flux and  $J_{\text{N}_2\text{O}_5}$ : another uncertainty in the calculated photolysis rates is due to uncertainties of the calculated actinic flux. In the mid- and upper stratosphere, uncertainties of the actinic flux are primarily due to the contribution of the direct solar

## Stratospheric limb measurements

L. Kritten et al.

Title Page

Abstract

Introduction

Conclusions

References

Tables

Figures

◀

▶

◀

▶

Back

Close

Full Screen / Esc

Printer-friendly Version

Interactive Discussion



**Stratospheric limb  
measurements**

L. Kritten et al.

Title Page

Abstract

Introduction

Conclusions

References

Tables

Figures

◀

▶

◀

▶

Back

Close

Full Screen / Esc

Printer-friendly Version

Interactive Discussion



irradiance rather than the contribution of scattered radiation from above or even from below (due to the absorption of ozone below 315 nm) for the altitude of interest (e.g., Madronich et al., 1985; Madronich, 1987; Bösch et al., 2003). Therefore, major uncertainties in the spectral actinic flux relevant for  $J_{\text{N}_2\text{O}_5}$  are primarily due to (a) the solar activity-dependent irradiance being particularly variable in the UV-C and UB-B spectral ranges, (b) overhead ozone, and (c) overhead  $\text{O}_2$ .

(a) In the UV-C and UV-A/B spectral ranges the spectral irradiance is known to be largely correlated with the solar activity (Foukal et al., 2006). Our measurements were conducted during the declining phase of solar cycle 23 in June 2005 with total solar sunspot numbers being around 30 (i.e. about 25 % of the maximum sunspot number of cycle 23 seen in 2001). Therefore, it is rather likely that the solar radiation in the UV-C and UV-A was not particularly elevated during our measurement (Foukal et al., 2006). Further, during balloon flights conducted in 1996 and 1997, we measured the actinic flux relevant for photolysis of  $\text{NO}_2$  in a similar descending phase solar cycle 22. No significant departure of the measured and modelled actinic fluxes was found (Bösch et al., 2003). Also, during three balloon flights conducted in 2003 and 2004, we measured the spectral solar irradiance. For the 325–370 nm spectral range reasonable agreement was found between our irradiance and the measurements of SIM, SCIAMACHY, SOLSPEC and Modtran 3.7 (within  $< 5\%$ ), indicating no abnormal increase in the spectral irradiance in the UV-A in 2003 and 2004 when the sunspot numbers were larger than in 2005 (Gurlit et al., 2005). In addition, recent solar irradiance measurements claim that from solar maximum to minimum, solar radiation in the extreme UV may decrease four to six times more than predicted by models (Haigh et al., 2010). Accordingly, we see no reason to assume that radiation in the UV-C was particularly elevated during our measurements, at least not in an amount to explain an increased  $s_1$  value.

(b) Ozone in the mid- and upper stratosphere used to scale the actinic flux was measured on several occasions during the same campaign. For our simulation overhead

ozone measured at high accuracy by solar occultation spectroscopy is used (e.g., Butz et al., 2006; Dorf et al., 2008).

(c) Further the total overhead airmass and thus  $O_2$  is determined by in-situ measured pressures and temperatures, and any significant departure would have been detected through a curved rather than straight line in a Langley plot of measured slant column amount of ozone (or BrO) vs. total air mass (e.g., see Fig. 2 in Dorf et al., 2008).

Finally, the impact of a potentially too coarse wavelength grid (1 nm) in calculation of  $J_{N_2O_5}$  (Eq. 1) should be very small because of the lack of differential structures in  $\sigma_{N_2O_5}(\lambda, T)$  (Trentmann et al., 2003). In conclusion, the error in the calculated  $J_{N_2O_5}$  due to uncertainties of the calculated actinic flux is assumed to be negligible.

The individual uncertainties and errors of our study on  $\sigma_{N_2O_5}(\lambda, T)$  are summarised in Table 1. In order to estimate a total error, we added positive and negative deviations separately in quadrature, even though we are aware that a monte carlo estimation would be more adequate, we used this approximation due to high computational costs of a Monte Carlo approach. The individual noise and forward model parameter errors add to a total error of +1.15 to -1.35 for  $s_1$  and +0.6 to -0.24 for  $s_2$ .

## 4 Implications

Now we relate our results concerning  $\sigma_{N_2O_5}(\lambda, T)$  to earlier discrepancies of measured and modelled  $N_2O_5$  in the stratosphere and assess possible Implications on global ozone. Previous inter-comparisons of measured and modelled  $N_2O_5$  in the stratosphere revealed the following:

(a) The studies of Brühl et al. (2007) and Funke et al. (2011) also addressed inter-comparisons of  $N_2O_5$  measured by ENVISAT/MIPAS. In particular for the retrieval from the IMK/IAA (Institut für Meteorologie und Klimaforschung and Instituto de Astrofísica de Andalucía) Brühl et al. (2007), stated a problem to reproduce the observed nighttime partitioning between  $N_2O_5$  and  $NO_2$  in the middle stratosphere using the recommended set of reaction coefficients and photolysis data, while for the Halloween solar proton

## Stratospheric limb measurements

L. Kritten et al.

Title Page

Abstract

Introduction

Conclusions

References

Tables

Figures

◀

▶

◀

▶

Back

Close

Full Screen / Esc

Printer-friendly Version

Interactive Discussion



event in late October 2003, the inter-comparison of measurements and model resulted in much larger model than measured  $\text{N}_2\text{O}_5$ , except for the KASIMA model Funke et al. (2011).

(b) At the same time, Wolff et al. (2008) stated a low bias ( $-0.25$  ppb) of ACE-FTS  $\text{N}_2\text{O}_5$  relative to the MIPAS IMK-IAA retrieval for the middle stratosphere around 30 km.

(c) Moreover, in a recent study, Wetzel et al. (2012) found slightly larger measured MIPAS-B  $\text{N}_2\text{O}_5$  concentrations than those modelled by EMAC (ECHAM/MESSy Atmospheric Chemistry) for the mid-stratosphere (22–34 km) at high latitudes during mid winter, i.e.  $\text{SZA} > 86^\circ$ .

More recent sensitivity studies using SLIMCAT (not shown) indicate that in order to reconcile modelled and measured  $\text{N}_2\text{O}_5$  for the studies mentioned in (a), the  $\text{N}_2\text{O}_5$  photolysis frequency would need to be increased by at least a factor 1.5 to 2 in the UV-B/A. However an increase in UV-B/A photolysis of  $\text{N}_2\text{O}_5$  by a factor 1.5 to 2 would deteriorate the existing agreement between  $\text{N}_2\text{O}_5$  concentrations measured by ACE-FTS and simulated by SLIMCAT for sunrise and sunset (finding b), but at the same time it would potentially increase the discrepancy found in the study of Wetzel et al. (2012). Finally, such an increase is not supported by the result of our study. Therefore, such an increase in the  $\text{N}_2\text{O}_5$  photolysis in the UV-B/A spectral range is neither supported by all, however contradicting field measurements, nor by the result of our study, or by the recommendation of JPL-2011.

A possible increase of  $\sigma_{\text{N}_2\text{O}_5}(\lambda, T)$  in the UV-C spectral range as indicated by the present study would not resolve the discrepancies found in (a), mainly since below 10 mbar the UV-C radiation rapidly contribute less and less to the  $\text{N}_2\text{O}_5$  photolysis as the altitude become lower. At the same time, it may not modify finding (b), and at best it would only slightly improve the mismatch found in (c).

Therefore, it is rather likely that the mismatch of the ENVISAT/MIPAS  $\text{N}_2\text{O}_5$  with the various model predictions is not due to an incorrect  $\sigma_{\text{N}_2\text{O}_5}(\lambda, T)$  used in the models, but due to any other reason.

## Stratospheric limb measurements

L. Kritten et al.

Title Page

Abstract

Introduction

Conclusions

References

Tables

Figures

◀

▶

◀

▶

Back

Close

Full Screen / Esc

Printer-friendly Version

Interactive Discussion



## Stratospheric limb measurements

L. Kritten et al.

Title Page

Abstract

Introduction

Conclusions

References

Tables

Figures

◀

▶

◀

▶

Back

Close

Full Screen / Esc

Printer-friendly Version

Interactive Discussion



In order to assess the consequences of our finding on global ozone, sensitivity simulations for the modified  $\sigma_{\text{N}_2\text{O}_5}(\lambda, T)$  were performed using the SLIMCAT 3-D CTM (e.g., Chipperfield, 1999, 2006). The model was run at a horizontal resolution of  $5.6^\circ \times 5.6^\circ$  with 32 levels between the surface and  $\sim 60$  km. The model was forced using European Centre for Medium-Range Weather Forecasts (ECMWF) ERA-Interim data and used the model's standard stratospheric chemistry scheme. A first run (run R) used JPL-2011 photochemical data. A second run (N) was identical to run R but used the updated values for  $\sigma_{\text{N}_2\text{O}_5}$  derived in this work. Run N was initialised from run R in July 2007 and integrated for 2 yr. Output from 2008 was used for this exercise.

Figure 8 shows the percentage change in annual mean  $\text{O}_3$ ,  $\text{NO}_2$  and  $\text{N}_2\text{O}_5$  between runs N and R for 2008, along with the  $\text{O}_3$  change in September.  $\text{N}_2\text{O}_5$  decreases above 30 km by up to 4 % in the annual (24 h) mean due to the increased photolysis at short wavelengths. Below 30 km (35 km near the poles)  $\text{N}_2\text{O}_5$  increases by up to 5 % due to the slower photolysis at longer wavelengths. The change in  $\text{NO}_2$  shows an opposite pattern reflecting the changing partitioning between  $\text{NO}_x$  and  $\text{N}_2\text{O}_5$ . Overall, the impact of the change in  $\sigma_{\text{N}_2\text{O}_5}$  on ozone is small. In the mid-stratosphere (30–35 km) the increased  $\text{NO}_x$ , which is the main sink of odd oxygen in this region, leads to an  $\text{O}_3$  decrease of about 0.25 % with the scaled  $\sigma_{\text{N}_2\text{O}_5}$ . Below 30 km the ozone response changes sign, consistent with the  $\text{NO}_x$  change, but it is still only around 0.25 %. In September  $\text{O}_3$  loss inside the polar vortex is suppressed slightly (−0.6 % change).

## 5 Summary and conclusion

For the first time the absorption cross-section of  $\text{N}_2\text{O}_5$   $\sigma_{\text{N}_2\text{O}_5}(\lambda, T)$  is constrained from measurements of the diurnal increase in  $\text{NO}_2$  in the tropical mid-stratosphere. It is found that in the UV-C (200–260 nm)  $\sigma_{\text{N}_2\text{O}_5}(\lambda, T)$  may be larger by a factor of  $1.6 \pm 0.8$ , and in the UVB/A (260–350 nm) smaller by a factor of  $0.9 \pm 0.26$  as compared to the JPL-2011 recommendations. Additional uncertainties of our study are due to uncertainties of the forward model parameters, which are estimated to be up to +0.6 to −0.9

in the UV-C and up to +0.6 to -0.3 in the UV-B/A. A total error is estimated to be +1.15 to -1.35 in the UV-C and +0.6 to -0.24 in the UV-B/A. The outcome of our study could be improved if other  $\text{NO}_y$  species (e.g., by MIPAS-B) were simultaneously measured. This was unfortunately not possible in a second joint attempt to simultaneously operate the MIPAS-B and mini-DOAS instrument in a joint deployment over North-Eastern Brazil 2008 due to technical constraints.

Overall, above 30 km  $\text{N}_2\text{O}_5$  concentrations decrease by up to 4 % in the annual (24 h) mean due to the increased photolysis at short wavelengths, when using the retrieved  $\sigma_{\text{N}_2\text{O}_5}(\lambda, T)$ . Below 30 km (35 km near the poles)  $\text{N}_2\text{O}_5$  increases by up to 5 % due to the slower photolysis at longer wavelengths. For this altitude region in some cases lower measured than modelled  $\text{N}_2\text{O}_5$  have been reported for the late morning lower stratosphere, which could be reconciled increasing  $\sigma_{\text{N}_2\text{O}_5}(\lambda, T)$  in the UV-B/A wavelength range by up to a factor of 2 compared to the JPL-2011 recommendations (e.g., as indicated by recent SLIMCAT runs). Increasing the  $\text{N}_2\text{O}_5$  photolysis in the UV-C according to our finding is not enough to eliminate the stated mismatch of measured and modelled  $\text{N}_2\text{O}_5$  for altitudes above 30 km. Therefore firm conclusions on a larger UV-C  $\text{N}_2\text{O}_5$  absorption cross section as indicated by our study can not be drawn from previous measurement vs. model inter-comparison studies.

Further a sensitivity test using our revised vs. the JPL-2011 recommended  $\sigma_{\text{N}_2\text{O}_5}(\lambda, T)$  show little effects on global ozone. Above 30 km, where UV-C light is strongly contributing to the  $\text{N}_2\text{O}_5$  photolysis, the increase in  $\sigma_{\text{N}_2\text{O}_5}(\lambda, T)$  ( $1.6 \pm 0.8$  in the  $w_1$  wavelength region), leads to an increase in  $\text{NO}_2$  and through R2 to 0.2 % less ozone at most. Below 30 km, where  $\text{N}_2\text{O}_5$  photolysis due to UVB/A light is more important, our smaller  $\sigma_{\text{N}_2\text{O}_5}(\lambda, T)$  ( $0.9 \pm 0.26$  in the  $w_2$  wavelength region) leads to slightly more ozone, i.e. 0.2 % in the mid-latitude stratosphere, and as much as 0.6 % in the 20–25 km region over the Antarctica in spring.

Finally our approach could also be used to retrieve more and other parameters from simultaneous atmospheric measurements of the relevant  $\text{NO}_y$  species, including a tighter assessment of the absorption cross-section of  $\text{NO}_2$ .

## Stratospheric limb measurements

L. Kritten et al.

Title Page

Abstract

Introduction

Conclusions

References

Tables

Figures

◀

▶

◀

▶

Back

Close

Full Screen / Esc

Printer-friendly Version

Interactive Discussion



## Stratospheric limb measurements

L. Kritten et al.

Title Page

Abstract

Introduction

Conclusions

References

Tables

Figures

◀

▶

◀

▶

Back

Close

Full Screen / Esc

Printer-friendly Version

Interactive Discussion



*Acknowledgements.* Funding for this study came from the Deutsche Forschungsgemeinschaft (DFG) (grants Pf 384/5-1/2, PF384/9-1/2), Deutsches Zentrum für Luft und Raumfahrt (DLR) (contracts BMWi 50EE0840), the European Union (EU) through the EU projects Reconcile (FP7-ENV-2008-1-226365), and SHIVA (FP7-ENV-2007-1-226224) and the European Space Agency (ESA) (contract ESA-ESRIN: No. RFQ/3-12092/07/I-435 OL). The SLIMCAT modelling was supported by the NERC National Centre for Atmospheric Science (NCAS), UK and we thank Wuhu Feng for his help. We thank the CNES equipe nacelles pointées and the balloon team from Aire sur l'Adour/France without which the balloon flight would not have been possible. We also thank our colleagues from the LPMA balloon team (P. Jeseck, I. Pepin and Y. Té) for the successful cooperation. Finally, we are grateful for the hospitality and support given by the personnel of the Instituto Nacional de Pesquisas Espaciais (INPE), Brazil to successfully perform the balloon flight at Teresina/Brazil. A. Butz is funded through the Emmy–Noether programme of the Deutsche Forschungsgemeinschaft (DFG) grant BU2599/1-1 (RemoteC).

## References

- Bösch, H., Camy-Peyret, C., Chipperfield, M. P., Fitzenberger, R., Harder, H., Platt, U., and Pfeilsticker, K.: Upper limits of stratospheric IO and OIO inferred from center-to-limb-darkening corrected balloon-borne solar occultation visible spectra: implications for total gaseous iodine and stratospheric ozone, *J. Geophys. Res.*, 108, 4455, doi:10.1029/2002JD003078, 2003. 4695, 4696, 4703
- Butz, A., Bösch, H., Camy-Peyret, C., Chipperfield, M., Dorf, M., Dufour, G., Grunow, K., Jeseck, P., Kühl, S., Payan, S., Pepin, I., Pukite, J., Rozanov, A., von Savigny, C., Sioris, C., Wagner, T., Weidner, F., and Pfeilsticker, K.: Inter-comparison of stratospheric O<sub>3</sub> and NO<sub>2</sub> abundances retrieved from balloon borne direct sun observations and Envisat/SCIAMACHY limb measurements, *Atmos. Chem. Phys.*, 6, 1293–1314, doi:10.5194/acp-6-1293-2006, 2006. 4695, 4704
- Brasseur, G. and Solomon, S.: *Aeronomy of the Middle Atmosphere*, Springer, P.O. Box 17, 3300 Dordrecht, the Netherlands, 2005. 4692
- Brühl, C., Steil, B., Stiller, G., Funke, B., and Jöckel, P.: Nitrogen compounds and ozone in the stratosphere: comparison of MIPAS satellite data with the chemistry climate model

## Stratospheric limb measurements

L. Kritten et al.

Title Page

Abstract

Introduction

Conclusions

References

Tables

Figures

◀

▶

◀

▶

Back

Close

Full Screen / Esc

Printer-friendly Version

Interactive Discussion



ECHAM5/MESSy1, *Atmos. Chem. Phys.*, 7, 5585–5598, doi:10.5194/acp-7-5585-2007, 2007. 4690, 4704

Chipperfield, M. P.: Multiannual simulations with a three-dimensional chemical transport model, *J. Geophys. Res.*, 104, 1781–1805, 1999. 4706

5 Chipperfield, M. P.: New version of the TOMCAT/SIMCAT off-line chemical transport model: intercomparison of stratospheric tracer experiments, *Q. J. Roy. Meteor. Soc.*, 132, 1179–1203, doi:10.1256/qj.05.51, 2006. 4695, 4697, 4706

Crutzen, P. J.: The influence of nitrogen oxides on the atmospheric ozone content, *Q. J. Roy. Meteor. Soc.*, 96, 320–325, 1970. 4690

10 Dorf, M., Butz, A., Camy-Peyret, C., Chipperfield, M. P., Kritten, L., and Pfeilsticker, K.: Bromine in the tropical troposphere and stratosphere as derived from balloon-borne BrO observations, *Atmos. Chem. Phys.*, 8, 7265–7271, doi:10.5194/acp-8-7265-2008, 2008. 4704

Deutschmann, T., Beirle, S., Frieß, U., Grzegorski, M., Kern, C., Kritten, L., Platt, U., Prados-Román, C., Pukite, J., Wagner, T., Werner, B., and Pfeilsticker, K.: The Monte Carlo atmospheric radiative transfer model McArtim: introduction and validation of Jacobians and 3-D features, *J. Quant. Spectrosc. Ra.*, 112, 1119–1137, doi:10.1016/j.jqsrt.2010.12.009, 2011. 4694, 4695

Foukal, P., Fröhlich, C., Spruit, H., and Wigley, T. M. L.: Variations in solar luminosity and their effect on the Earth's climate, *Nature*, 443, 161–166, doi:10.1038/nature05072, 2006. 4703

20 Funke, B., Baumgaertner, A., Calisto, M., Egorova, T., Jackman, C. H., Kieser, J., Krivolutsky, A., López-Puertas, M., Marsh, D. R., Reddmann, T., Rozanov, E., Salmi, S.-M., Sinnhuber, M., Stiller, G. P., Verronen, P. T., Versick, S., von Clarmann, T., Vyushkova, T. Y., Wieters, N., and Wissing, J. M.: Composition changes after the "Halloween" solar proton event: the High Energy Particle Precipitation in the Atmosphere (HEPPA) model versus MIPAS data intercomparison study, *Atmos. Chem. Phys.*, 11, 9089–9139, doi:10.5194/acp-11-9089-2011, 2011. 4690, 4704, 4705

25 Gebhardt, C., Rozanov, A., Hommel, R., Weber, M., Bovensmann, H., Burrows, J. P., Densten, D., Froidevaux, L., and Thompson, A. M.: Stratospheric ozone trends and variability as seen by SCIAMACHY from 2002 to 2012, *Atmos. Chem. Phys.*, 14, 831–846, doi:10.5194/acp-14-831-2014, 2014. 4689

30 Gurlit, W., Bösch, H., Bovensmann, H., Burrows, J. P., Butz, A., Camy-Peyret, C., Dorf, M., Gerilowski, K., Lindner, A., Noël, S., Platt, U., Weidner, F., and Pfeilsticker, K.: The UV-A and visible solar irradiance spectrum: inter-comparison of absolutely calibrated, spectrally

Stratospheric limb  
measurements

L. Kritten et al.

Title Page

Abstract

Introduction

Conclusions

References

Tables

Figures

◀

▶

◀

▶

Back

Close

Full Screen / Esc

Printer-friendly Version

Interactive Discussion



medium resolution solar irradiance spectra from balloon- and satellite-borne measurements, Atmos. Chem. Phys., 5, 1879–1890, doi:10.5194/acp-5-1879-2005, 2005. 4703

Haigh, J. D., Winning, A. R., Toumi, R., Harder, J. W.: An influence of solar spectral variations on radiative forcing of climate, Nature, 467, 696–699, doi:10.1038/nature09426, 2010. 4703

5 Harwood, M. H., Jones, R. L., Cox, R. A., Lutman, E., and Rattigan, O. V.: Temperature-dependent absorption cross-sections of N<sub>2</sub>O<sub>5</sub>, J. Photochem. Photobio. A., 73, 167–175, 1993. 4695

Harwood, M. H., Burkholder, J. B., and Ravishankara, A. R.: Photodissociation of BrONO<sub>2</sub> and N<sub>2</sub>O<sub>5</sub>: Quantum Yields for NO<sub>3</sub> Production at 248, 308, and 352.5 nm, J. Phys. Chem. A, 102, 1309–1317, 1998.

10 IPCC: Climate Change 2007: The Physical Science Basis. Contribution of Working Group I to the Fourth Assessment Report of the Intergovernmental Panel on Climate Change, edited by: Solomon, S., Qin, D., Manning, M., Chen, Z., Marquis, M., Averyt, K. B., M. Tignor and Miller, H. L., Cambridge University Press, Cambridge, UK, New York, NY, USA, 2007. 4690

15 Johnston, H. S.: Reduction of stratospheric ozone by nitrogen oxide catalysts from supersonic transport exhaust, Science, 173, 517–522, 1971. 4690

Jones, E. J. and Wulf, O. I.: The absorption coefficient of nitrogen pentoxide in the ultraviolet and the visible absorption spectrum of NO<sub>3</sub>, J. Chem. Phys., 5, 873–877, 1937. 4692

20 Kritten, L., Butz, A., Dorf, M., Deutschmann, T., Köhl, S., Prados-Roman, C., Pukite, J., Rozanov, A., Schofield, R., and Pfeilsticker, K.: Time dependent profile retrieval of UV/vis absorbing radicals from balloon-borne limb measurements – a case study on NO<sub>2</sub> and O<sub>3</sub>, Atmos. Meas. Tech., 3, 933–946, doi:10.5194/amt-3-933-2010, 2010. 4692, 4693, 4694, 4695, 4701

25 Lary, D. J. and Pyle, J. A.: Diffusive radiation, twilight and photochemistry, J. Atmos. Chem., 13, 373–392, 1991. 4695

Madronich, S.: Photodissociation in the atmosphere. 1. Actinic flux and the effects of ground reflections and clouds, J. Geophys. Res., 92, 9740–9752, 1987. 4703

Madronich, S., Hastie, D. R., Schiff, H. I., and Ridley, B. A.: Measurements of the photodissociation coefficient of NO<sub>2</sub> in the atmosphere, II. Stratospheric measurements, J. Atmos. Chem., 3, 233–245, 1985. 4703

30 Oh, D., Sisk, W., Young, A., and Johnston, H.: Nitrogen dioxide fluorescence from N<sub>2</sub>O<sub>5</sub> photolysis, Chem. Phys., 85, 7146–7158, 1986. 4696

**Stratospheric limb  
measurements**

L. Kritten et al.

Title Page

Abstract

Introduction

Conclusions

References

Tables

Figures

◀

▶

◀

▶

Back

Close

Full Screen / Esc

Printer-friendly Version

Interactive Discussion



- Osborne, B. A., Marston, G., Kaminski, L., Jones, N. C., Gingell, J. M., Mason, N. J., Walker, I. C., Delwiche, J., and Hubin-Franskin, M.-J.: Vacuum ultraviolet spectrum of dinitrogen pentoxide, *J. Quant. Spectrosc. Ra.*, 64, 67–74, 2000.
- 5 Park, S., Croteau, P., Boering, K. A., Etheridge, D. M., Ferretti, D., Fraser, P. J., Kim, K.-R., Krummel, P. B., Langenfelds, R. L., van Ommen, T. D., Steele, L. P., and Trudinger, C. M.: Trends and seasonal cycles in the isotopic composition of nitrous oxide since 1940, *Nat. Geosci.*, 5, 261–265, doi:10.1038/ngeo1421, 2012. 4690
- Platt, U., and Stutz, J.: *Differential Optical Absorption Spectroscopy (DOAS), Principle and Applications*, Springer Verlag, Heidelberg, 2008. 4694
- 10 Ravishankara, A. R., Daniel, J. S., and Portmann, R. W.: Nitrous oxide (N<sub>2</sub>O): the dominant ozone-depleting substance emitted in the 21st century, *Science*, 326, 123–125, 2009. 4689
- Rodgers, C. D.: *Inverse Methods for Atmospheric Sounding*, World Scientific, Singapore, New Jersey, London, Hongkong, 2000. 4694, 4699, 4700, 4701
- Sander, S., Friedl, R. R., Barkern, J., Golden, D., Kurylo, M., Wine, P., Abbat, J., Burkholder, J., Moortgart, C., Huie, R., and Orkin, R. E.: Chemical kinetics and photochemical data for use in atmospheric studies, Technical Report, NASA/JPL Publication, Jet Propulsion Laboratory, Pasadena, 17, 2011. 4689, 4690, 4695, 4696, 4702, 4715
- 15 Trentmann, J., Bovensmann, H., Eyring, V., Mueller, R., and Burrows, J. P.: Impact of accurate photolysis calculations on the simulation of stratospheric chemistry, *J. Atmos. Chem.*, 44, 225–240, 2003. 4704
- Weidner, F., Bösch, H., Bovensmann, H., Burrows, J. P., Butz, A., Camy-Peyret, C., Dorf, M., Gerilowski, K., Gurlit, W., Platt, U., von Friedeburg, C., Wagner, T., and Pfeilsticker, K.: Balloon-borne limb profiling of UV/vis skylight radiances, O<sub>3</sub>, NO<sub>2</sub>, and BrO: technical set-up and validation of the method, *Atmos. Chem. Phys.*, 5, 1409–1422, doi:10.5194/acp-5-1409-2005, 2005. 4694
- 25 Wetzel, G., Oelhaf, H., Ruhnke, R., Friedl-Vallon, F., Kleinert, A., Kouker, W., Maucher, G., Reddmann, T., Seefeldner, M., Stowasser, M., Trieschmann, O., von Clarmann, T., and Fischer, H.: NO<sub>y</sub> partitioning and budget and its correlation with N<sub>2</sub>O in the Arctic vortex and in summer mid-latitudes in 1997, *J. Geophys. Res.*, 107, 4280, doi:10.1029/2001JD000916, 2002. 4697
- 30 Wetzel, G., Oelhaf, H., Kirner, O., Friedl-Vallon, F., Ruhnke, R., Ebersoldt, A., Kleinert, A., Maucher, G., Nordmeyer, H., and Orphal, J.: Diurnal variations of reactive chlorine and ni-

## Stratospheric limb measurements

L. Kritten et al.

Title Page

Abstract

Introduction

Conclusions

References

Tables

Figures

◀

▶

◀

▶

Back

Close

Full Screen / Esc

Printer-friendly Version

Interactive Discussion



trogen oxides observed by MIPAS-B inside the January 2010 Arctic vortex, *Atmos. Chem. Phys.*, 12, 6581–6592, doi:10.5194/acp-12-6581-2012, 2012. 4705

Wiegele, A., Kleinert, A., Oelhaf, H., Ruhnke, R., Wetzell, G., Friedl-Vallon, F., Lengel, A., Maucher, G., Nordmeyer, H., and Fischer, H.: Spatio-temporal variations of NO<sub>y</sub> species in the northern latitudes stratosphere measured with the balloon-borne MIPAS instrument, *Atmos. Chem. Phys.*, 9, 1151–1163, doi:10.5194/acp-9-1151-2009, 2009. 4697

WMO (World Meteorological Organization): Scientific Assessment of Ozone Depletion: 2010, Global Ozone Research and Monitoring Project-Report No. 52, 516 pp., Geneva, Switzerland, 2011. 4690

WMO (World Meteorological Organization), Press Release No. 934, available at: [http://www.wmo.int/pages/mediacentre/press\\_releases/pr\\_934\\_en.html](http://www.wmo.int/pages/mediacentre/press_releases/pr_934_en.html), 2014. 4690

Wolff, M. A., Kerzenmacher, T., Strong, K., Walker, K. A., Toohey, M., Dupuy, E., Bernath, P. F., Boone, C. D., Brohede, S., Catoire, V., von Clarmann, T., Coffey, M., Daffer, W. H., De Mazière, M., Duchatelet, P., Glatthor, N., Griffith, D. W. T., Hannigan, J., Hase, F., Höpfner, M., Huret, N., Jones, N., Jucks, K., Kagawa, A., Kasai, Y., Kramer, I., Küllmann, H., Kuttippurath, J., Mahieu, E., Manney, G., McElroy, C. T., McLinden, C., Mébarki, Y., Mikuteit, S., Murtagh, D., Piccolo, C., Raspollini, P., Ridolfi, M., Ruhnke, R., Santee, M., Senten, C., Smale, D., Tétard, C., Urban, J., and Wood, S.: Validation of HNO<sub>3</sub>, ClONO<sub>2</sub>, and N<sub>2</sub>O<sub>5</sub> from the Atmospheric Chemistry Experiment Fourier Transform Spectrometer (ACE-FTS), *Atmos. Chem. Phys.*, 8, 3529–3562, doi:10.5194/acp-8-3529-2008, 2008. 4705

Yao, F., Wilson, I., and Johnston, H.: Temperature-dependent ultraviolet absorption spectrum for dinitrogen pentoxide, *J. Phys. Chem.*, 86, 3611–3615, 1982.

Stratospheric limb  
measurements

L. Kritten et al.

Title Page

Abstract

Introduction

Conclusions

References

Tables

Figures

I◀

▶I

◀

▶

Back

Close

Full Screen / Esc

Printer-friendly Version

Interactive Discussion

**Table 1.** Uncertainties in the retrieval of  $s_1$  and  $s_2$ .

|       | Retrieved Value | Noise | NO <sub>y</sub> Initialisation | O <sub>3</sub> Initialisation | $\sigma_{\text{NO}_2}$ | $k_{\text{NO}+\text{O}_3}$ | total       |
|-------|-----------------|-------|--------------------------------|-------------------------------|------------------------|----------------------------|-------------|
| $s_1$ | 1.6             | ±0.80 | +0.5,−0.3                      | +0.3,−0.40                    | +0.5,−0.6              | +0.6,−0.9                  | +1.15,−1.35 |
| $s_2$ | 0.9             | ±0.26 | +0.1,−0.2                      | +0.3,−0.2                     | +0.3,−0.3              | +0.6,−0.3                  | +0.6,−0.24  |

Stratospheric limb  
measurements

L. Kritten et al.

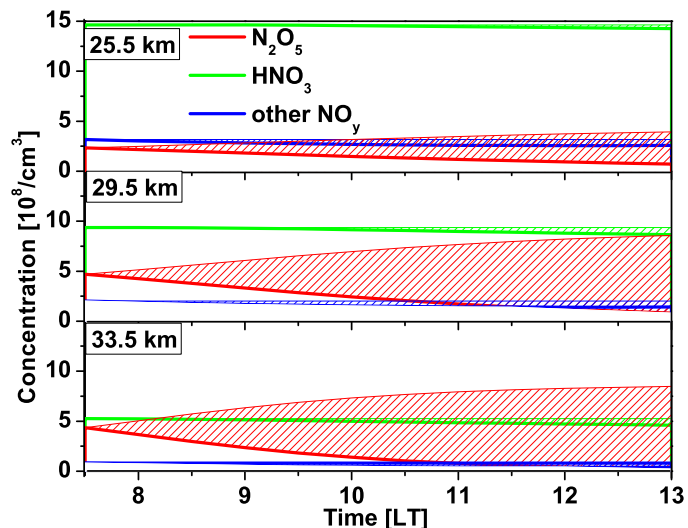


**Fig. 1.** Temporal evolution of  $\text{N}_2\text{O}_5$  (red),  $\text{HNO}_3$  (green) and the sum of other  $\text{NO}_y$  species ( $\text{ClONO}_2 + \text{HO}_2\text{NO}_2 + \text{BrONO}_2$ , blue) for different altitudes of the tropical mid-stratosphere ( $5.1^\circ\text{S}$ ,  $43.6^\circ\text{W}$ ). The lower boundary of the striped area denotes the temporal evolution of the particular gas, and the striped area shows the total amount of  $\text{NO}_x$ , which is released by photolysis from the considered  $\text{NO}_y$  species. Note that the release from  $\text{N}_2\text{O}_5$  is double due to two N atoms.

[Title Page](#)[Abstract](#)[Introduction](#)[Conclusions](#)[References](#)[Tables](#)[Figures](#)[I◀](#)[▶I](#)[◀](#)[▶](#)[Back](#)[Close](#)[Full Screen / Esc](#)[Printer-friendly Version](#)[Interactive Discussion](#)

## Stratospheric limb measurements

L. Kritten et al.

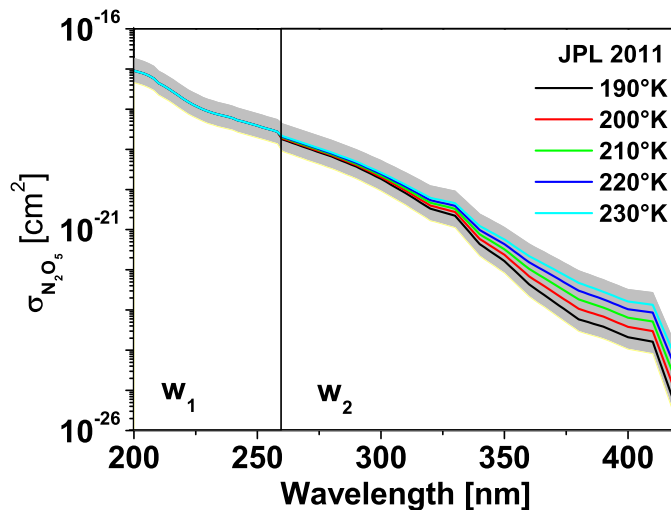


**Fig. 2.** Absorption cross-section and uncertainty (grey area) of  $\sigma(\lambda, T)$  as recommended by JPL 2011  $\text{N}_2\text{O}_5$  (Sander et al., 2011). For this study,  $\sigma_{\text{N}_2\text{O}_5}(\lambda, T)$  is divided into two wavelength regions  $w_1$  and  $w_2$ . No temperature dependence of  $\sigma_{\text{N}_2\text{O}_5}(\lambda, T)$  is reported for  $w_1$ , the  $T$  dependence for  $w_2$  is indicated by different colours.

[Title Page](#)[Abstract](#)[Introduction](#)[Conclusions](#)[References](#)[Tables](#)[Figures](#)[◀](#)[▶](#)[◀](#)[▶](#)[Back](#)[Close](#)[Full Screen / Esc](#)[Printer-friendly Version](#)[Interactive Discussion](#)

Stratospheric limb  
measurements

L. Kritten et al.

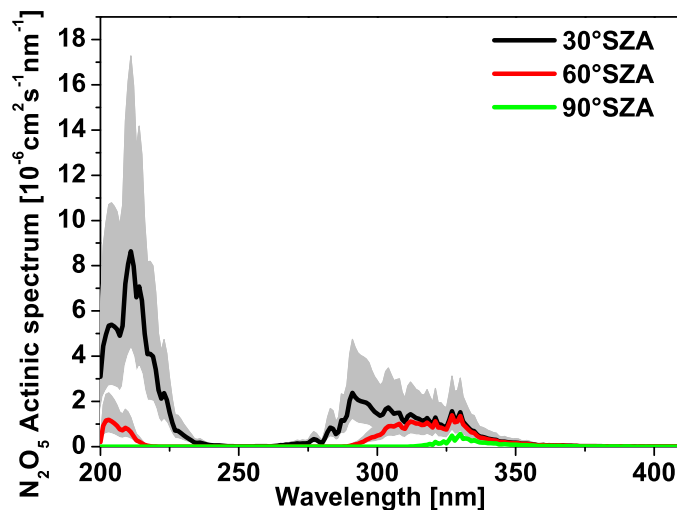


**Fig. 3.** Actinic spectrum of  $\text{N}_2\text{O}_5$  i.e., the product of  $\sigma_{\text{N}_2\text{O}_5}(\lambda, T)$  (at 230 K) and modelled actinic fluxes for an overhead ozone column of 283 Dobson Units, and different SZAs at 30.5 km.

[Title Page](#)[Abstract](#)[Introduction](#)[Conclusions](#)[References](#)[Tables](#)[Figures](#)[◀](#)[▶](#)[◀](#)[▶](#)[Back](#)[Close](#)[Full Screen / Esc](#)[Printer-friendly Version](#)[Interactive Discussion](#)

## Stratospheric limb measurements

L. Kritten et al.

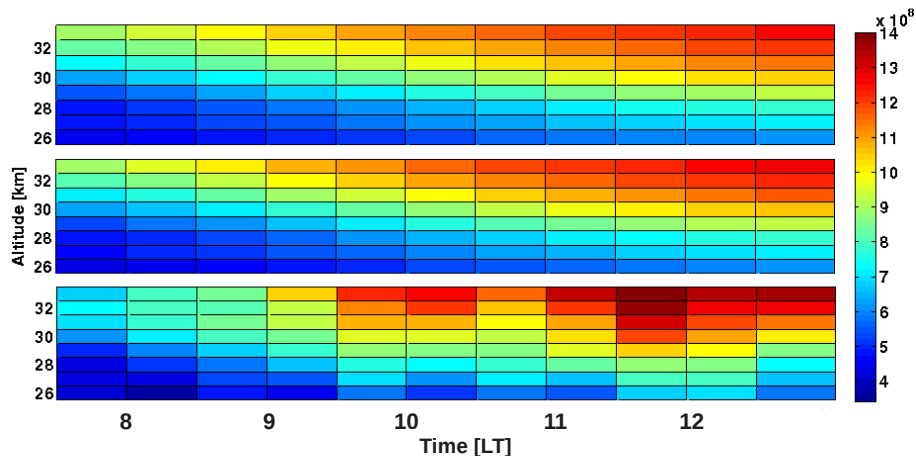


**Fig. 4.** Temporal evolution of the  $\text{NO}_2$  concentration in the tropical mid-stratosphere ( $5.1^\circ \text{S}$ ,  $43.6^\circ \text{W}$ ) for 13 June 2005, modelled using the JPL-2011 recommendation for  $\sigma_{\text{N}_2\text{O}_5}(\lambda, T)$  i.e.,  $s_1 = 1.0$  and  $s_2 = 1.0$  (upper panel), using the inferred  $s_1 = 1.6$  and  $s_2 = 0.9$  (middle panel). The measured  $\text{NO}_2$  concentration is shown in the lower panel. Units are given in  $\text{molec cm}^{-3}$ .

Title Page

Abstract

Introduction

Conclusions

References

Tables

Figures

◀

▶

◀

▶

Back

Close

Full Screen / Esc

Printer-friendly Version

Interactive Discussion



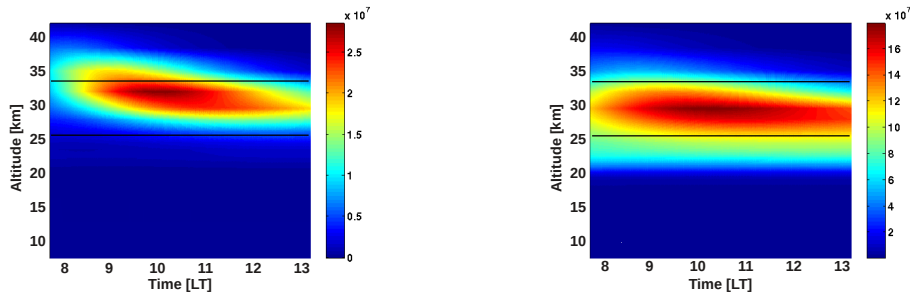


**Fig. 5.** Sensitivity of the  $\text{NO}_2$  concentration in our model to the scaling factors  $s_1$  (left panel) and  $s_2$  (right panel) on the absorption cross-section of  $\text{N}_2\text{O}_5$ . Units are given in  $\text{molec cm}^{-3}$ . The altitude region used for the analysis is marked by black lines.

Stratospheric limb measurements

L. Kritten et al.

Title Page

Abstract Introduction

Conclusions References

Tables Figures

◀ ▶

◀ ▶

Back Close

Full Screen / Esc

Printer-friendly Version

Interactive Discussion



Stratospheric limb  
measurements

L. Kritten et al.

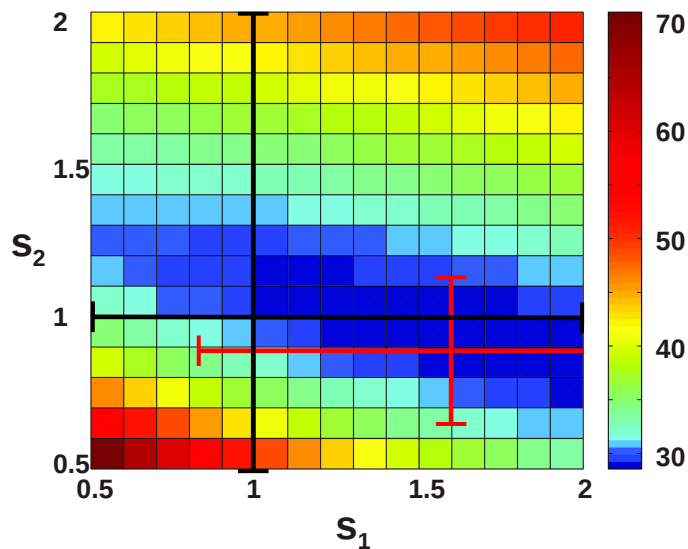


**Fig. 6.**  $\chi^2$  as a function of  $s_1$  and  $s_2$ , as given in Eq. (9). The inferred global minimum is shown in red together with the total error due to noise error of the retrieval. The corresponding JPL-2011 values are given in black.

[Title Page](#)[Abstract](#)[Introduction](#)[Conclusions](#)[References](#)[Tables](#)[Figures](#)[◀](#)[▶](#)[◀](#)[▶](#)[Back](#)[Close](#)[Full Screen / Esc](#)[Printer-friendly Version](#)[Interactive Discussion](#)

Stratospheric limb  
measurements

L. Kritten et al.

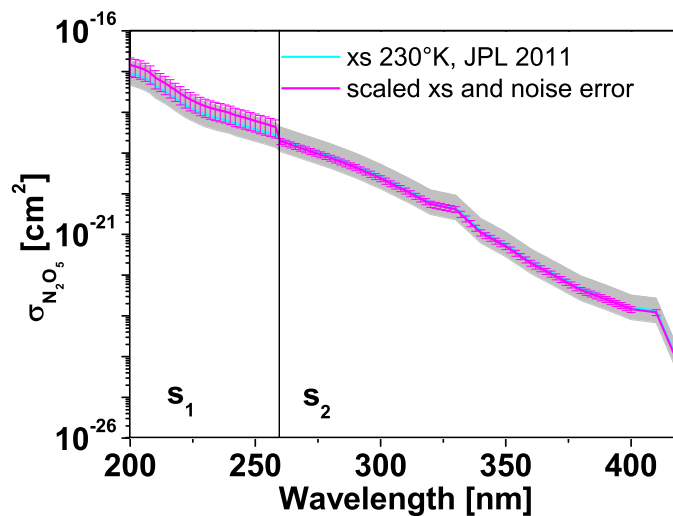


**Fig. 7.**  $\sigma_{\text{N}_2\text{O}_5}(\lambda, T)$  measured in the laboratory (JPL-2011, shown in light blue) and inferred in the present study (shown in pink).

[Title Page](#)[Abstract](#)[Introduction](#)[Conclusions](#)[References](#)[Tables](#)[Figures](#)[◀](#)[▶](#)[◀](#)[▶](#)[Back](#)[Close](#)[Full Screen / Esc](#)[Printer-friendly Version](#)[Interactive Discussion](#)

## Stratospheric limb measurements

L. Kritten et al.

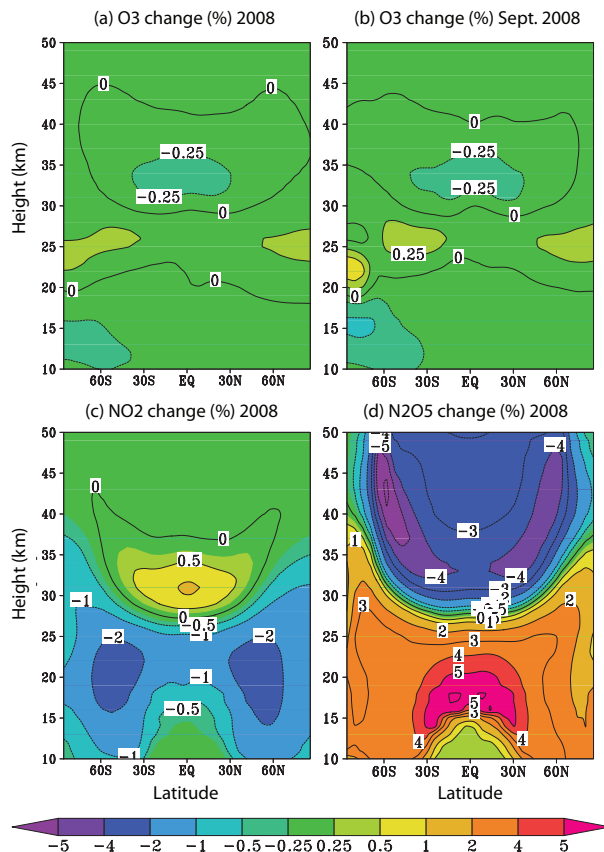


**Fig. 8.** Difference in zonal mean fields (%) for 2008 from the run of the SLIMCAT 3-D CTM with scaled  $J_{\text{N}_2\text{O}_5}$  (run N) minus the run with recommended JPL-2011 kinetics (run R) for **(a)** annual mean O<sub>3</sub>, **(b)** September mean O<sub>3</sub>, **(c)** annual mean NO<sub>2</sub>, and **(d)** annual mean N<sub>2</sub>O<sub>5</sub>. Note irregular contour interval.